

## Supporting Information

### **An organic transistor matrix for scalable intracellular action potential recording.**

Yasutoshi JIMBO (1), Daisuke SASAKI (2), Takashi OHYA (3), Sunghoon LEE (1), Wonryung LEE (1), Faezeh ARAB HASSANI (1), Tomoyuki YOKOTA (1), Katsuhisa MATSUURA (2), Shinjiro UMEZU (3), Tatsuya SHIMIZU (2), Takao SOMEYA\* (1)

1. Department of Electrical Engineering and Information Systems, Graduate School of Engineering, The University of Tokyo, 7-3-1 Hongo, Bunkyo-ku, Tokyo 113-8656, Japan
2. Institute of Advanced Biomedical Engineering and Science, Tokyo Women's Medical University, 8-1 Kawada-Cho, Shinjuku-Ku, Tokyo 162-8666, Japan
3. Graduate School of Creative science and Engineering, Waseda University, 3-4-1 Okubo, Shinjuku-ku, Tokyo 169-8555, Japan

\* All correspondence should be sent to [someya@ee.t.u-tokyo.ac.jp](mailto:someya@ee.t.u-tokyo.ac.jp)

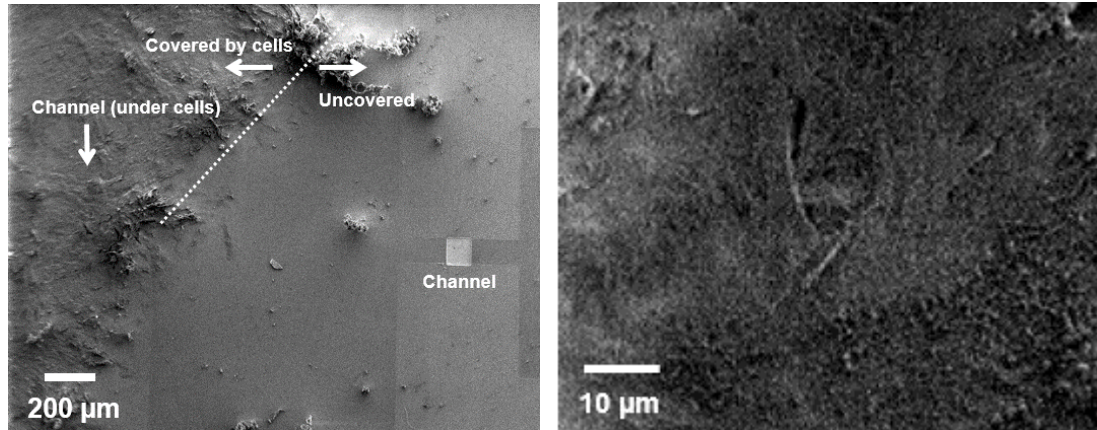


Fig. S1. Scanning electron microscopy (SEM) image of cells on the channel of OECTs. The left image shows the boundary of the region covered by cells and uncovered region. Cells form a tight sheet, and thus the OECT is not visible when it is covered. Right image shows a high-magnification image of the cell sheet.

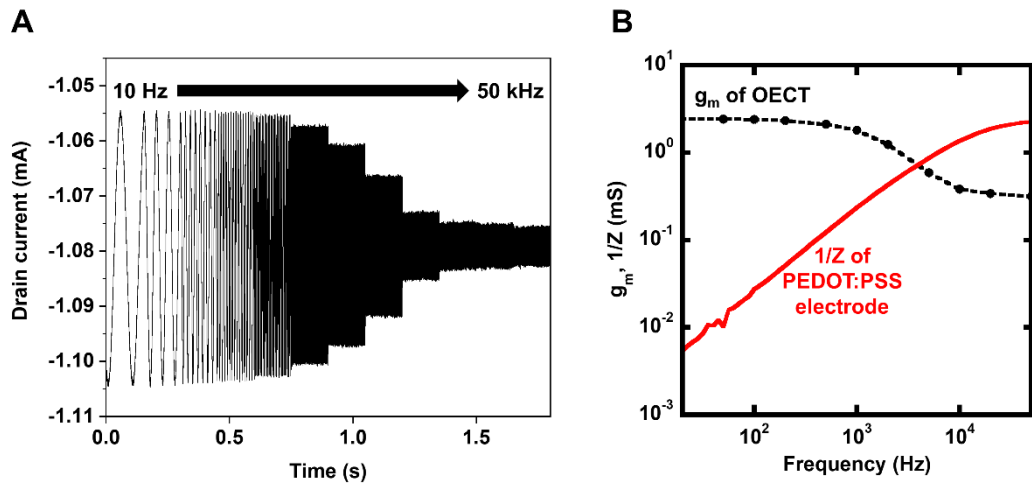


Fig. S2. Frequency response of OECT. (A) Drain current of an OECT while sine waves ( $20 \text{ mV}_{pp}$ ) were applied to the gate electrode. Frequency was varied from 10 Hz to 50 kHz for each 0.15 s, and the amplitude of the output current decreased accordingly. (B) Comparison with a PEDOT:PSS electrode of the same scale. Regarding voltage as input and current as output,  $g_m$  of OECT and  $1/Z$  of PEDOT:PSS are plotted in the same figure. OECT has a higher output to low frequency input.

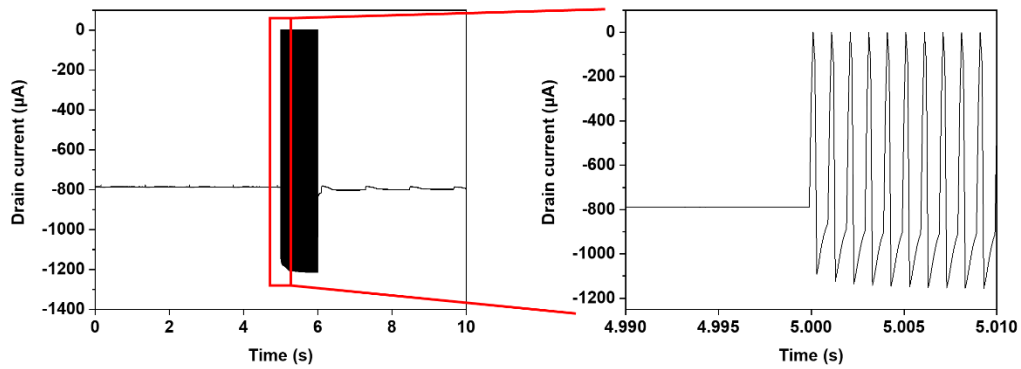


Fig. S3. Waveform of the drain current while a pulse voltage was applied to the drain electrode.

Applied pulse made a round trip between  $-600$  mV for  $0.75$  ms and  $0$  V for  $0.25$  ms with a rising time of  $0.25$   $\mu$ s. The waveform does not show square shape because of undershoot and delayed response. It should be noted that the sampling rate was  $10$  kHz, so that the number of the data point was  $10$  for  $1$  cycle and the sharpness of peaks are possibly exaggerated.

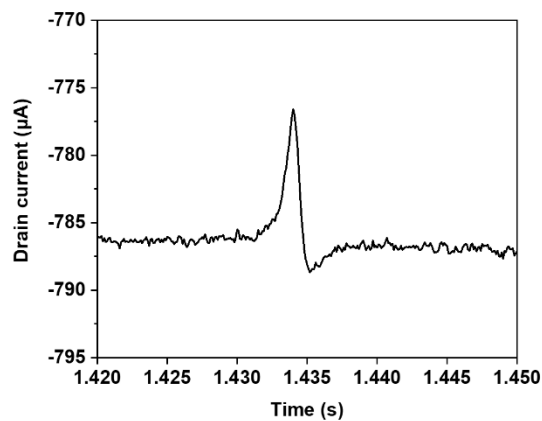


Fig. S4. Magnified figure of the recorded peak before the pulse input.

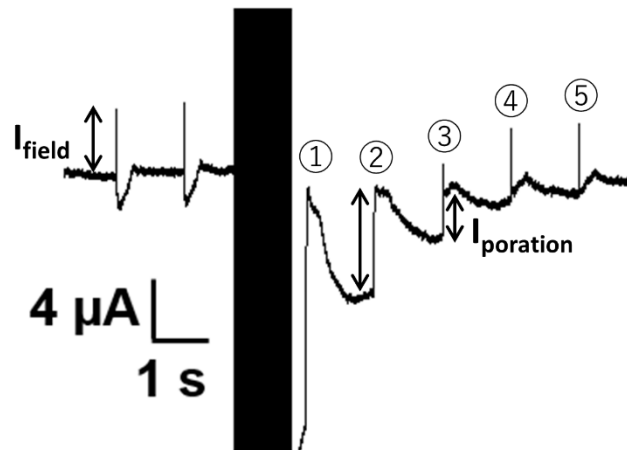


Fig. S5. Example of the procedure to count peaks and measure the amplitude of the induced peaks.

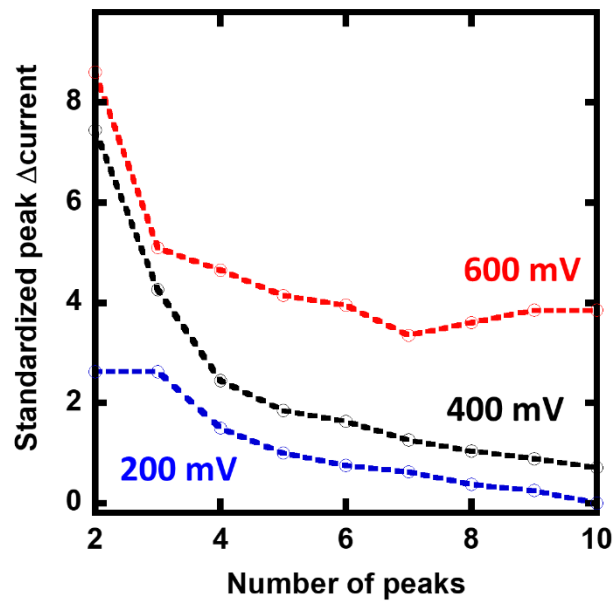


Fig. S6. The effect of the applied drain voltage on the duration and amplitude of the induced peaks. An OEET with a channel size of  $100 \times 100 \mu\text{m}^2$  was used for plotting this

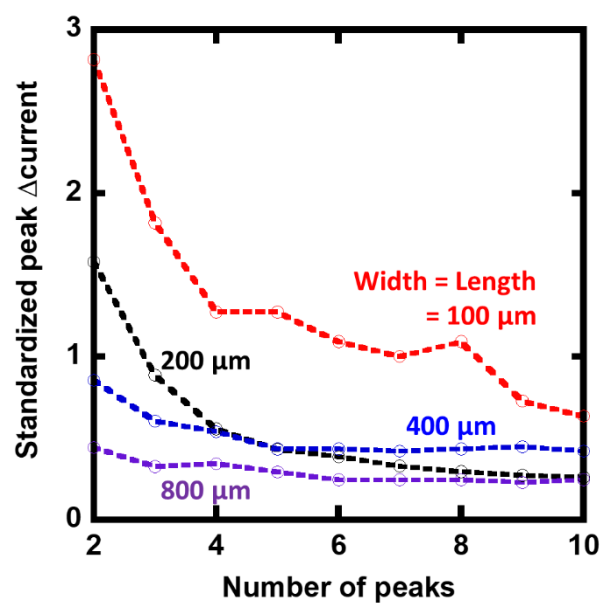


Fig. S7. Duration and amplitude of induced peaks versus variable channel sizes. Compared to Fig. 4B, this sample has a larger overlap (100  $\mu$ m) between Au drain/source electrode and the PEDOT:PSS channel.

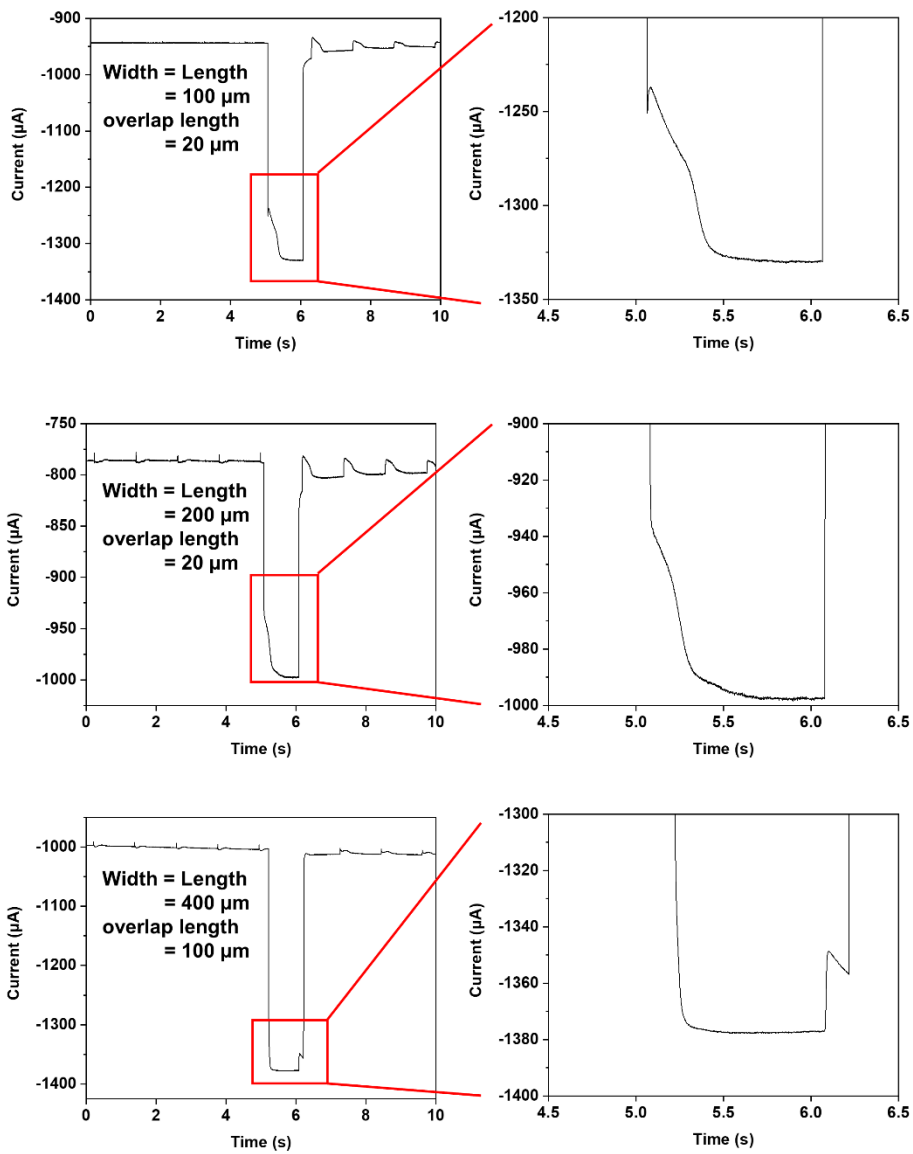


Fig. S8. Electroporation-induced peaks overlapped with the undershoot current during the cyclic pulse input. The amplitude of the drain-source voltage and pulse was 600 mV. The amplitude of peaks recorded during the input is larger than that recorded after the input.

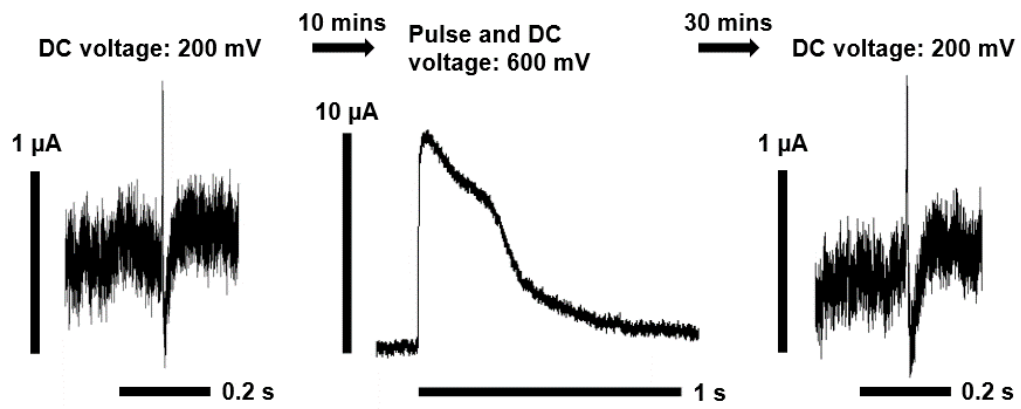


Fig. S9. Effect of intracellular action potential recording using electroporation on the field potential recorded after sufficient rest time.



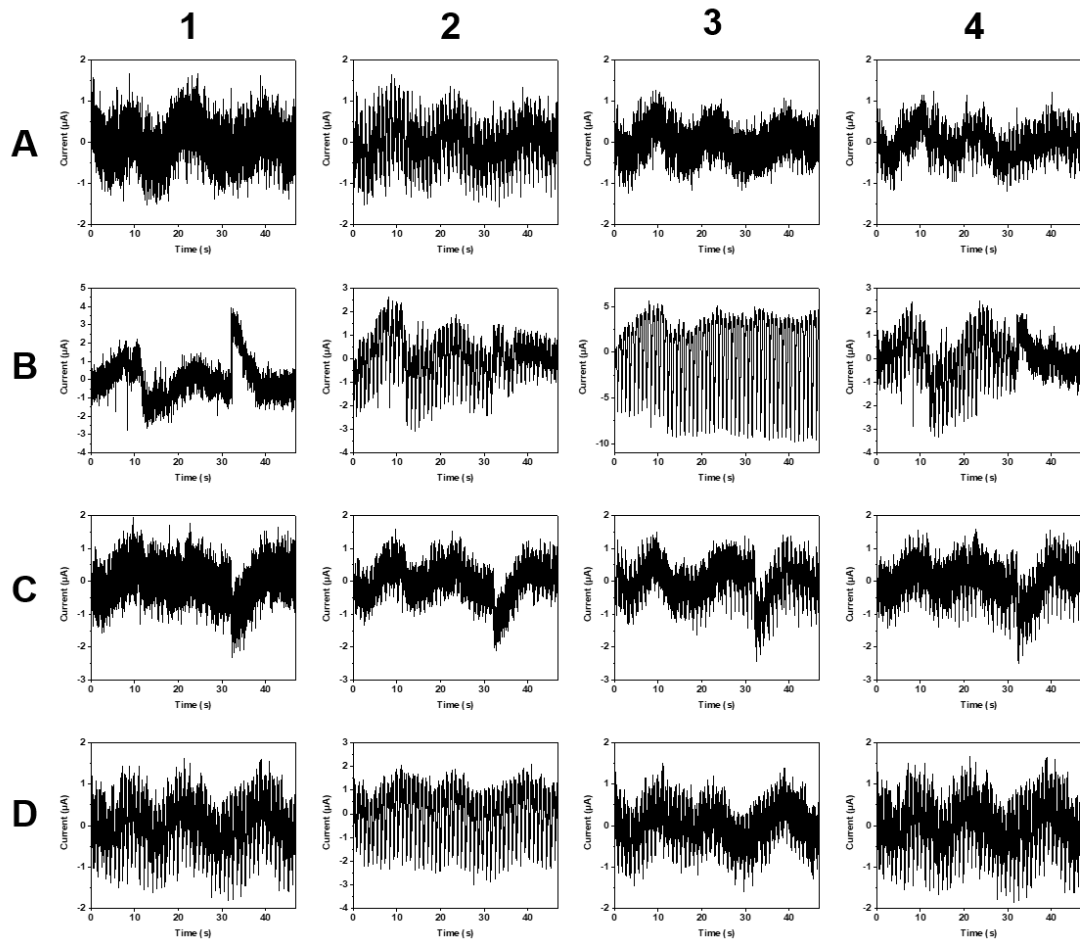


Fig. S10. Action potential mapping recorded by a 4×4 OECT matrix. Data used in figure 5 are displayed with a longer time window. Most of sensors such as (B-3) continuously recorded peaks, but some sensors such as (B-2) and (B-4) recorded smaller signal or failed recording after 30 seconds.

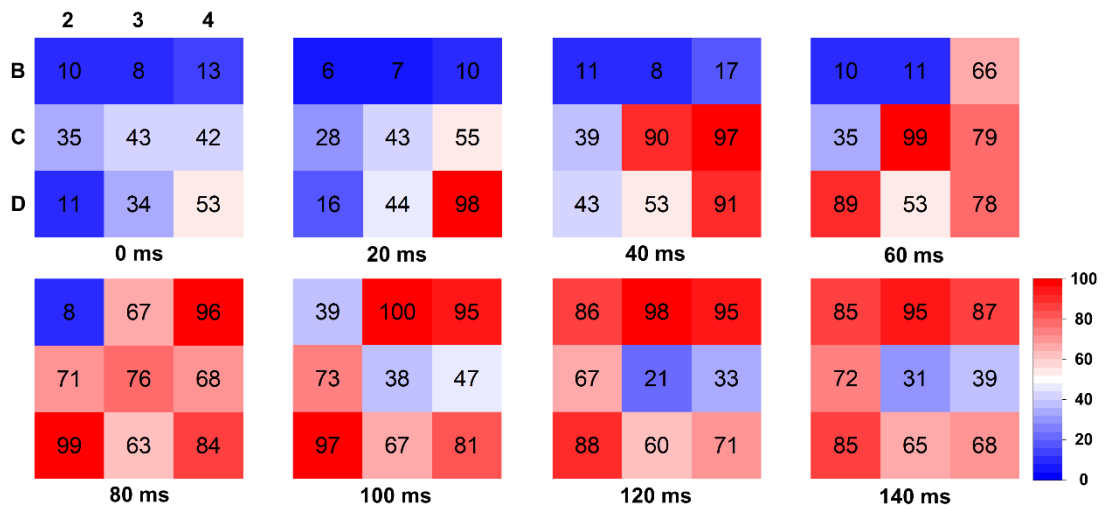


Fig. S11. Heat map showing the propagation of cardiac potential recorded by  $4 \times 4$  OECT matrix.

Recorded potentials are standardized to 0 - 100 scale: the minimum and maximum value recorded

in the pixel corresponds to 0 and 100, respectively. 0 ms in the figure corresponds to 0.86 s in Fig.

5C. Scan line A and data line 1 was omitted because most of cell did not catch any signal.

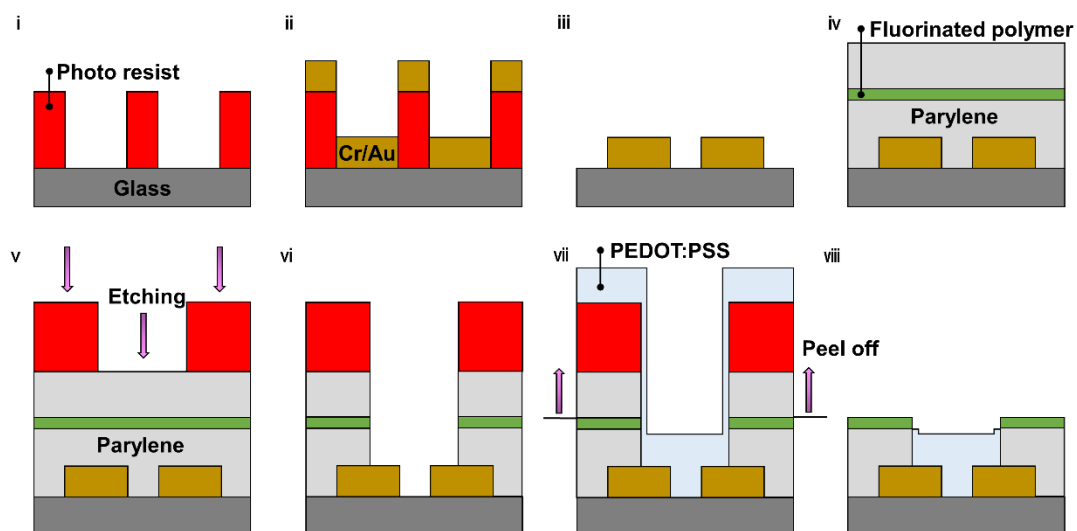


Fig. S12. Schematic illustration of the fabrication process for a single OEET. Au electrode was patterned by a liftoff process (i-iii), and the entire surface was covered with a double parylene layer sandwiching a fluorinated polymer (iv). Then, the PEDOT:PSS channel was patterned by a physical peel-off of the sacrificial second parylene layer (v-viii).

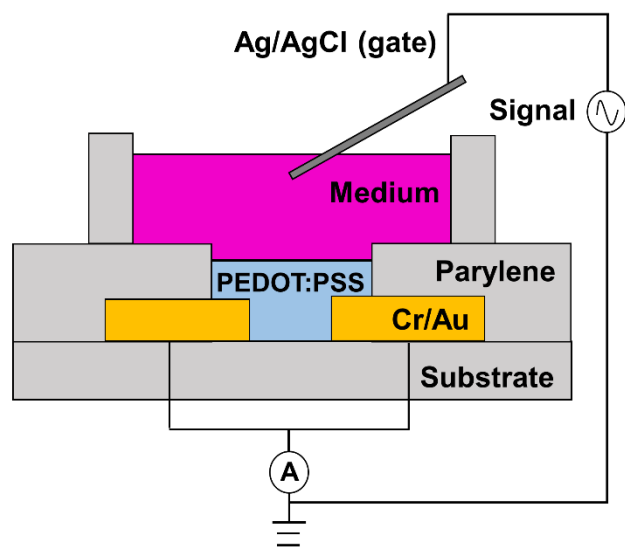


Fig. S13. PEDOT:PSS electrode configured by shorting the drain and source electrode of an OECT.

Table S1. Interval of action potential peaks before and after the pulse input.

|          | Width, Length<br>( $\mu\text{m}$ ) | Overlap<br>( $\mu\text{m}$ ) | Interval (s)<br>(Before) | Interval (s)<br>(After) |
|----------|------------------------------------|------------------------------|--------------------------|-------------------------|
| Sample 1 | 100                                | 20                           | 1.17                     | 1.18                    |
| Sample 2 | 200                                | 20                           | 1.19                     | 1.19                    |
| Sample 3 | 400                                | 20                           | 1.26                     | 1.24                    |
| Sample 4 | 800                                | 20                           | 1.18                     | 1.18                    |
| Sample 5 | 100                                | 100                          | 1.14                     | 1.14                    |
| Sample 6 | 200                                | 100                          | 1.12                     | 1.16                    |
| Sample 7 | 400                                | 100                          | 1.19                     | 1.16                    |
| Sample 8 | 800                                | 100                          | 1.14                     | 1.18                    |

Table S2. Comparison between this work and the exiting microelectrode arrays for intracellular recordings. Please note that it is difficult to make an exact comparison although they are summarized here. For example, one research used HL-1 cells and another used hiPSC-derived cardiomyocytes. Also, to calculate the success rate of intracellular access, one research considered all pixels, another ignored pixels which is not covered by cells, and another counted the number of wells containing multiple sensors instead of the number of pixels.

|   | Surface structure   | Voltage for stimulation | Other input for stimulation | Success rate of Intracellular access | Local amplifier | Matrix | Fabrication platform  |
|---|---------------------|-------------------------|-----------------------------|--------------------------------------|-----------------|--------|---|
| H. Hayes, <i>et al.</i> , 2019. [26]      | Planar              | $\pm 1$ V               | -                           | >90 % of 42 wells                    | -               | No     | Commercial device (Axion BioSystems, Inc.)                                    |
| B. Desbiolles, <i>et al.</i> , 2019. [24] | 3D nanovolcano      | -                       | -                           | 6 out of 21 pixels                   | -               | No     | Low temperature process (<135 °C) featuring ion beam etching                  |
| J. Abbott, <i>et al.</i> , 2017. [23]     | 3D nanopillar array | $\pm 1.2$ V             | -                           | >30 % (1024 pixels)                  | CMOS            | Yes    | Fabricated on CMOS manufactured by Taiwan Semiconductor Manufacturing Company |
| M. Dipalo, <i>et al.</i> , 2018. [33]     | Planar (Porous Pt)  | -                       | Laser sweep                 | >3500 out of 4096 pixels             | CMOS            | Yes    | Fabricated on commercial CMOS (3Brain AG)                                     |
| This work                                 | Planar (PEDOT:PSS)  | 0.6 V                   | -                           | 6 out of 16 pixels                   | OEET            | Yes    | Low temperature process (<140 °C)   |